Drug Delivery and Translational Research (2024) 14:329–341
https://doi.org/10.1007/s13346-023-01400-0

ORIGINAL ARTICLE

Evaluation of microstructure, dissolution rate, and oral bioavailability of paclitaxel poloxamer 188 solid dispersion

Yao Liu[1] · Yong Zhang[1] · Qiuli Yan[1] · Xueping Zhong[1] · Chunhui Hu[2]

Accepted: 21 July 2023 / Published online: 14 August 2023

Abstract

Poor solubility is a major challenge for enhancing the oral bioavailability and clinical application of many drugs, including the broad-spectrum chemotherapy drug paclitaxel (PTX). A practical approach to improving the solubility of insoluble drugs is through the use of solid dispersion (SD). This study aimed to investigate the potential of the triblock copolymer, poloxamer 188 (P188), as a carrier for preparing solid dispersion of paclitaxel using spray drying technology. We systematically studied its microstructure, dissolution behavior in vitro, and pharmacokinetics. Our findings demonstrate that PTX exists in an amorphous state in copolymer composed of polyoxyethylene-polyoxypropylene-polyoxyethylene (PEO-PPO-PEO) P188, with stronger miscibility with hydrophobic PPO segments. All three in vitro dissolution models revealed that the release rate of drugs in SD was significantly higher compared to that of physical mixtures (PM) as well as raw drugs. Furthermore, our pharmacokinetic results showed that the area under the curve(AUC) of PTX in SD was 6 times higher than that of active pharmaceutical ingredient(API), 4.5 times higher than PM, and the highest blood drug concentration (Cmax) reached 357.51 ± 125.54 (ng/mL), approximately 20 times higher than API. Overall, our findings demonstrate that the dissolution rate of amorphous PTX in SD significantly improves, effectively enhancing the oral bioavailability of PTX.

Keywords Solid dispersion · Microstructure · Drug polymer molecular interactions · Dissolution rate · Oral bioavailability

Introduction

Paclitaxel (PTX) is a complex chemical compound with a large molecular weight, produced in the bark of *Taxus chinensis* and is used to treat various types of cancers, including ovarian, breast, gastric, uterine, and non-small cell carcinoma [1–4]. It is currently used as a broad-spectrum chemotherapeutic agent [5]. However, due to its poor water solubility (about 5.56×10^{-3} g/L) and low oral bioavailability, less than 10% of the drug is excreted through the urine, rendering it a biopharmaceutics classification system (BCS) class IV drug [5]. Several drug delivery systems, such as solid dispersions [6], micelles [7], and nanoparticles [8], have been developed to improve its solubility. Still, only a few have been clinically approved, including Abraxane® (injection of suspension albumin-bound paclitaxel) and Lipusu® (paclitaxel liposomes for injection) [9]. However, the need for injection can cause low patient compliance, and studies have suggested that adverse effects can be slowed down with oral administration compared to injection administration [10]. Therefore, researchers have focused on developing an oral formulation for PTX, and one such formulation, DHP107, is currently undergoing clinical trials [10, 11].

The concept of solid dispersion was first proposed by Sekiguchi in 1961 and has since been widely used to enhance the dissolution rate and oral bioavailability of poorly soluble drugs [12]. Many subsequent investigators found that the solid dispersion (SD) technique was applied to improve the solubility and dissolution rate of other poorly soluble drugs [13]. Poloxamers are a type of triblock copolymer composed of polyoxyethylene-polyoxypropylene-polyoxyethylene (PEO-PPO-PEO) that act as linkers between PEO segments, with PPO segments present in an hydrophobic state, and PEO segments in a hydrophilic morphology. Several studies have demonstrated the efficacy of poloxamer188 (P188) as a carrier in SD to improve the solubility and dissolution rate

✉ Chunhui Hu
chunhuihu@qhu.edu.com

[1] Medical College, Qinghai University, Xining, 810001 Qinghai, People's Republic of China

[2] State Key Laboratory of Plateau Ecology and Agriculture, Qinghai University, Xining, 810001 Qinghai, People's Republic of China

of drugs, such as cefuroxime axetil, sulfadiazine, sulfaisoxazole, and carvedilol [14–16]. Our group's previous studies have also shown significant improvement in the dissolution rate of drugs during SD prepared by poloxamers, and we systematically studied their microstructure and solubilization mechanism [17, 18].

In this study, we aimed to improve the oral bioavailability of PTX by preparing a solid dispersion of paclitaxel-poloxamer 188 (PTX/P188-SD) using the spray drying technique. To investigate the interaction forces between the drug and polymers, we employed differential scanning calorimetry (DSC), Fourier transform infrared spectroscopy (FT-IR), and ^{1}H-nuclear magnetic resonance (^{1}H-NMR). We also evaluated the micromorphology of the SD formulations using powder X-ray diffraction (PXRD) and scanning electron microscopy (SEM). To examine the in vitro dissolution kinetics, we utilized intrinsic dissolution, powder dissolution, and pH conversion two-step dissolution. Finally, pharmacokinetic studies were performed in Wistar rats to validate the ability of the SD formulation to improve oral bioavailability. This study sheds light on the potential influence of the interaction between PTX and P188 on drug dissolution, laying a theoretical foundation for the development of a new oral PTX preparation that enhances its oral bioavailability.

Materials and methods

Materials

Paclitaxel, docetaxel, and PEO-PPO-PEO triblock copolymer poloxamer188, polyethylene glycol as well as polypropylene glycol (purity > 98%) were obtained from Beijing Coupling Technology Co., Ltd. (Beijing, China). High-performance liquid chromatography (HPLC) grade methanol and dichloromethane (analytical grade) were purchased from Merck Co., Ltd. (Darmstadt, Germany). Buffer salts and other reagents of analytical grade were obtained from Tianjin Damao chemical reagent Technology Co., Ltd. (Tianjin, China). The chemical structures of model drugs and polymer materials used in the experiment are illustrated in Fig. 1.

Preparation of SDs and physical mixing (PM)

A mixture of PTX/P188 (w/w, 30/70) was dissolved in dichloromethane at a total concentration of 5 wt%, and this resulting solution was added to a Yamato spray dryer (ADL 311S, Yamato Scientific Company, Ltd.). The operation of this spray dryer included an inlet temperature of 52 °C, an outlet temperature of 30 °C, a solution feed rate of 5 mL/min, and an atomizing N_2 pressure of 0.1 MPa. After spray drying, the SDs were dried under a vacuum for at least 24 h and stored in a desiccator at room temperature. Pure PTX and pure P188 were prepared in the same manner.

The physical mixture of PTX and P188 (PTX-P188-PM) was prepared by sieving and mixing the two sample powders to ensure uniform mixing.

Physicochemical characterization

Powders X-ray diffraction (PXRD)

The pure PTX (in crystalline and amorphous form), P188, PTX/P188-PM, and PTX/P188-SD powders were characterized using an ESCALAB™ XI + X'pert powder X-ray diffractometer (ESCALAB™ XI + , MA, USA) with a voltage of 40 kV and a current of 200 mA. The samples were

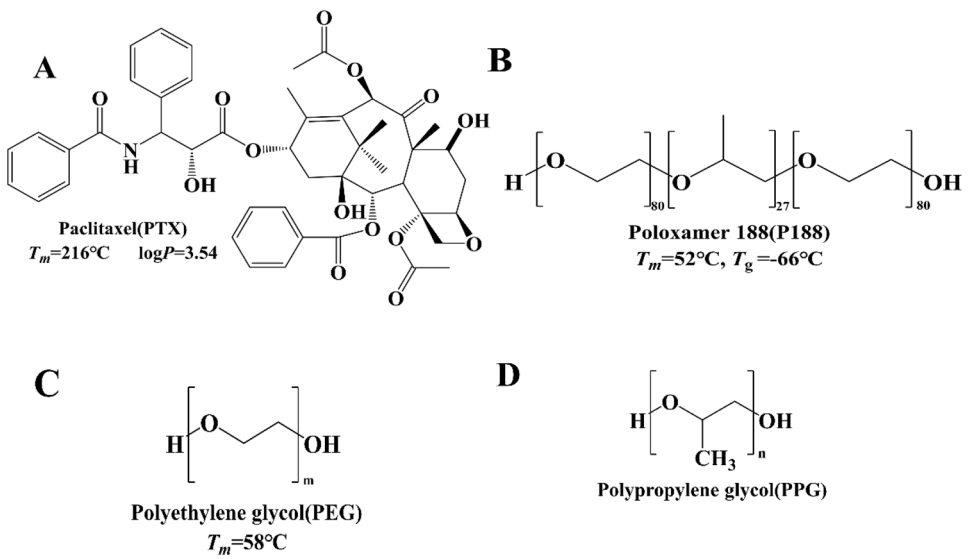

Fig. 1 Structures of **A** paclitaxel, **B** poloxamer 188, **C** polyethylene glycol, and **D** polypropylene glycol

scanned from $2\theta = 5$ to 35° at a scanning speed of 1°/min and a step size of 0.01°.

Scanning electron microscopy (SEM)

The microstructure and surface morphology of the solid dispersion powder was assessed using a scanning electron microscope (Merlin Compact, Germany) at an excitation voltage of 10 kV. Samples were placed on a copper platform and coated with gold for 180 s prior to observation.

Differential scanning calorimetry (DSC)

The melting point (T_m) was determined using a STA449F3-DSC200F3 (Netzsch, Germany). Briefly, 5–10 mg samples were loaded into pin-holed crimped aluminum pans. The sample was heated from 20 to 240 °C at a rate of 10 °C/min. The glass transition temperature (T_g) of SDs was determined by heating from 20 to 100 °C and cooling the sample from 100 to − 80 °C, followed by heating from − 80 to 240 °C at a rate of 20 °C/min.

Drug-polymer interaction

Fourier transform infrared spectroscopy (FT-IR)

To determine the contributions of functional groups in compounds related to drug-polymer interactions, IR spectra of SDs were collected using FT-IR spectroscopy (Nicolet 6700, Thermo Electron Corporation, USA) with a spectral resolution of 4 cm^{-1}. The wavenumbers of IR spectra ranging between 4000 and 500 cm^{-1} were recorded for further comparison. Prior to testing, the samples were placed at room temperature and vacuum dried for 24 h to limit the influence of moisture on the measurement.

Solution ^{1}H-nuclear magnetic resonance (^{1}H-NMR)

To investigate the molecular mechanism of drug-polymer interaction, the drugs, P188, and the various drugs loading SDs were dissolved in deuterochloroform, and their ^{1}H-NMR spectra were obtained at room temperature using an AVANCE NEO 600 (Bruker BioSpin GmbH, Rheinstetten, Germany). The deuterochloroform solvent signal was used as the reference ($CDCl_3$, 77.160 ppm). Spectral assignments for PTX and P188 were performed according to literature reports.

Hansen solubility parameters of drug and polymer

The Hansen solubility parameter method is commonly used for predicting drug-polymer miscibility and can be based on the calculated solubility parameters ($\Delta\delta_p$), which determines the compatibility between molecules based on the difference [19]. The interaction parameters were calculated using cohesive energy density (Eq. 1). The total solubility parameters of drugs and polymers can be calculated using Eq. 2. The group contribution method (Eq. 3) is used to calculate the partial solubility parameters of a substance.

$$\delta = (CED)^{0.5} = \left(\Delta E_V / V_m\right)^{0.5} \tag{1}$$

$$\delta_t = \delta_d^2 + \delta_p^2 + \delta_h^2 \tag{2}$$

$$\delta_d = \frac{\Sigma F_d}{V}; \delta_p \frac{\sqrt{\Sigma F_p^2}}{V}; \delta_h = \sqrt{\frac{\Sigma E_h}{V}} \tag{3}$$

where ΔE_v is the evaporation energy; V_m is the molar volume of the substance; δ_p, δ_h, and δ_d represent the solubility parameters of dispersion, polarity, and hydrogen bonding; F_d is the molar absorption constant of the dispersion group; F_p is the molar absorption constant of the polar group; E_h is the hydrogen bonding energy; and V is the molar volume of the substance.

Determination of the drug-polymer Flory–Huggins interaction parameter

To determine the solubility of the crystalline drug in polymers, an annealing method developed by Yu et al. [20] was employed. Briefly, drug-polymer mixtures were annealed at various temperatures to achieve phase equilibrium and scanned by DSC to detect residual drug crystals. For a drug-polymer mixture annealed at different temperatures, the method yields the upper and lower bounds of its equilibrium solution temperature. The Flory–Huggins model was utilized to obtain the drug-polymer interaction parameters. The drug activity at a given solubility can be calculated using Eq. 4, and the drug-polymer interaction parameter can be calculated through the Flory–Huggins model shown in Eq. 5. A DSC scanning method was employed to determine the following parameters.

$$\ln\alpha_d = \Delta H_m / R\left(1/T_m - 1/T\right) \tag{4}$$

$$\ln\alpha_d = \ln\Phi_d + (1 - 1/x)\Phi_p + \chi\Phi_p^2 \tag{5}$$

where α_d is the drug activity, T_m is the melting temperature of the pure drug, ΔH_m is the molar heat of fusion of the pure drug, T is the solubility temperature, Φ_d is the volume fraction of the drug, Φ_p is the volume fraction of the polymer, x is the molar volume ratio of the polymer and the drug, and χ is the drug-polymer interaction parameter.

Dissolution kinetics in vitro

In vitro dissolution kinetics is a critical pharmaceutical parameter for SD, reflecting whether the prepared SD can improve the oral bioavailability of poorly soluble drugs [21]. In this study, we evaluated the dissolution behavior using intrinsic dissolution, powder dissolution, and pH conversion two-step dissolution methods.

The concentration of PTX was determined using high-performance liquid chromatography (HPLC) (Agilent 1260 Series, Palo Alto, USA) with UV detection at 227 nm. We used a Diamonsil C18 column (4.6 × 150 mm, 5 μm), with methanol/water (70/30, v/v) as the mobile phase and a flow rate of 1.00 mL/min. The column temperature was 30 °C, and the injection volume was 10.00 μL. The HPLC method was validated for specificity, calibration curve, precision, repeatability, stability, and recovery.

Intrinsic dissolution rate (IDR) of SDs

To compare the IDR of PTX, PM, and SDs, we utilized a previously developed intrinsic dissolution method [22]. Briefly, raw PTX (crystalline and amorphous), PM, and SDs were compacted into sharp cylindrical tablets (11 mm diameter and ~ 2 mm thickness). The tablets weighed 80 mg and had a tablet hardness of 5 Kgf (measured using a tablet hardness tester). The resulting tablets were placed into syringe tubes using paraffin, and a single surface was exposed to 20 mL of a dissolution medium in a 400 mL beaker with a stir bar stirring at 100 rpm ($n = 3$). The dissolution medium consisted of 0.01 M HCl (pH = 1.4), with the temperature maintained at 37 °C. At 0.5-min intervals, 0.3 mL of the solution was removed and centrifuged at 15,000 rpm for 3 min, double diluted with methanol, and assayed for the drug. The concentration of the drug was determined by HPLC.

Powder dissolution of SDs

The dissolution profile of the formulations (in powder form) was determined under non-sink conditions using a ZRS-8G dissolution apparatus (Tianjin Jingtuo Instrument Technology Co., Ltd, China). The dissolution medium consisted of 900 mL of PBS (pH = 7.4) containing 0.1% Tween 80, and the dissolution lasted for 1 h. The dissolution conditions included paddle stirring at 75 rpm; temperature of 37 °C; and sampling time points 5, 10, 15, 20, 30, 45, and 60 min. The solution was removed, centrifuged at 15,000 rpm for 3 min, double diluted with methanol, and assayed for drug presence. The concentration of the drug was determined through HPLC.

pH conversion two-step dissolution of SDs

The dissolution profile of the formulations (tablets) was determined under non-sink conditions using a ZRS-8G dissolution apparatus (Tianjin Jingtuo Instrument Technology Co., Ltd, China). The dissolution medium was 300 mL of 0.05 M HCl (pH = 1.4) containing 0.1% Tween 80, and the treatment lasted 1 h. The pH was then adjusted to 6.5 by adding 250 mL of 0.1 M Na_2HPO_4 solution. The dissolution test was then continued for an additional 4 h. Dissolution conditions included paddle stirring at 75 rpm, a temperature of 37 °C; sampling time points, 30, 60, 75, 90, 120, 180, 240, and 300 min. The solution was removed, centrifuged at 15,000 rpm for 3 min, double diluted with methanol, and assayed for drug presence. The PTX concentration was determined via HPLC/UV.

Pharmacokinetic comparison in wistar rat

Wistar rats ($n = 10$) weighing 180 ± 20 g, half male and half female, were used to evaluate the in vivo pharmacokinetics. The rats were fasted overnight before each administration and were fed 4 h after administration. The PTX, SDs, and PM were administered by gavage at a dose of 50 mg/kg. The jugular vein catheter was surgically placed 1 day before administration for systemic blood sampling. Blood samples of 200–400 μL were collected at 0.25, 0.5, 0.75, 1, 2, 4, 6, 8, 12, and 24 h after administration and were centrifuged at 13,000 rpm for 5 min. The upper plasma was stored at − 80 °C until testing.

After melting the plasma samples, 100 μL was taken, and an equal volume of mass spectrometry-grade dichloromethane was added. The sample was vortexed for 3 min and centrifuged at 4000 rpm for 5 min. Then, 1 mL of the lower liquid was taken and evaporated to dryness using nitrogen gas. Afterward, it was dissolved in 150 μL of methanol and combined with 10 μL of docetaxel (DTX) internal standard solution. The sample was vortexed for 3 min and centrifuged at 15,000 rpm for 10 min. The supernatant was obtained, and the sample content was determined using UPLC-HR-ESI-MS.

Our pharmacokinetic study of rats was conducted according to the standards recommended by the *Guidelines for the Care and Use of Laboratory Animals* (Animal Laboratory Resources Institute, 1995) and was approved by the Institutional Animal Care and Use Committee of Qinghai University.

UPLC-HR-ESI-MS analysis

The plasma concentrations of PTX were determined using a Dionex Ultimate 3000 RSLC system (Thermo Fisher) equipped with an ACQUITY UPLC BEH C18 Column

(130 Å, 2.6 µm, 150 mm × 2.1 mm) at a column temperature of 30 °C. The mobile phase consisted of eluent A (HPLC grade acetonitrile with 0.1% FA) and eluent B (water with 0.1% FA) and was delivered in a gradient elution mode as follows: 0–1 min, 50%B; 1–3 min, 50–10%; 3–4 min, 10%B; 4–5 min, 10–0%B; 5–6 min, 0%B; 6–7 min, 0–50%B; and 7–10 min, 50%B at a flow rate of 0.3 mL/min.

The MS analysis was performed using a Q-Orbitrap MS coupled with heated electrospray ionization (HESI). The auxiliary, sheath, and sweep gas flow rates were set at 35, 10, and 1 (arbitrary unit), respectively. The MS analysis was performed in full MS-ddMS^2 mode, with the damping gas in the C-trap, and nitrogen was used to stabilize the spraying. The auxiliary gas heater and capillary were set and maintained at 350 °C and 320 °C, respectively. In the negative mode, a spray voltage of 3.0 kV and an S-lens RF level of 60 V were used. The maximum injection time was 50 ms, and the automatic gain control target was set at 3.0 e^6. The full MS-ddMS^2 scan range was from 150.0000 to 1500.0000 m/z, and the precise molecular weight $[M\text{-}H]^+$ was used for qualitative analysis. The corresponding peak area was used for quantitative analysis, and the MS^2 fragments were used for further qualitative analysis.

Statistical analysis

SPSS 22.0 software was used to perform statistical analysis. The measurement data were expressed as mean ± standard deviation. The comparison of multiple samples was analyzed through ANOVA, with a significance level of $P < 0.01$. Figures were created using GraphPad Prism 8.3.0 software. The pharmacokinetic parameters were assessed through non-compartment model analysis using DAS 3.2.8.

Results and discussion

Characterization of PTX/P188-SD

PTX, PM, SD, and P188 underwent powder X-ray diffraction (PXRD) analysis. As shown in Fig. 2A, PTX demonstrated characteristic diffraction peaks at 5.5°, 8.8°, and 12.7° [23], indicating a crystalline state. The PTX treated with spray drying was amorphous, and the only characteristic diffraction peaks of P188 appeared at 19.2° and 23.3° after physical mixing. In SD, no diffraction peaks were observed for PTX, but only the diffraction peak of P188 was detected, suggesting that PTX existed in an amorphous form within the polymer.

To further demonstrate the morphology of the drug in SD, we analyzed the melting point (T_m) and glass transition temperature (T_g) of the drug using differential scanning calorimetry (DSC) (Fig. 2B). The results showed that crystalline PTX exhibited an endothermic peak at 215.5 °C. In contrast, SDs showed an endothermic peak at 52 °C, corresponding to the T_m of PTX and P188, respectively. The amorphous state of PTX exhibited a typical s-shaped step pattern change at 148.5 °C, indicating the T_g [24]. When analyzing SDs, a unique T_g appeared at − 24 °C (data not shown), consistent with the T_g theoretically calculated by the Gordon-Taylor model. These results indicate that PTX exists in an amorphous form in P188, and the whole system is homogeneous. Since P188 is a triblock copolymer composed of PEO-PPO-PEO, the PPO segments in the amorphous state are arranged between the PEO sheets in the crystalline state. Based on the results of PXRD and DSC, we speculate that the drug is mainly distributed in the PPO segments of P188, ensuring good compatibility between PTX and P188, which will be confirmed by the following theoretical calculations and experimental tests.

SEM was used to observe the surface morphology of the samples. Crystalline PTX showed a fibrous surface that was rough and fluffy (Fig. 2Ca, Ce), while amorphous PTX appeared lumpy with a smooth surface (Fig. 2Cb, Cf). In contrast, SD (Fig. 2C, Cg) showed no fibrils, and the surface resembled that of P188 (Fig. 2 Cd, Ch), further confirming the existence of PTX in an amorphous state.

Drug-polymer interaction

The FT-IR analysis mainly examined the chemical bond or functional group vibrational absorption in the PTX and P188 molecules to determine their interaction. The carbonyl C = O (1721 cm^{-1}) and amide CO–NH (1652.89 cm^{-1}) characteristic absorption of PTX were used to assess the intermolecular interaction between PTX and P188, with the CO–NH stretching showing a more significant change [25]. PM analysis revealed that the CO–NH absorption peak on PTX did not exhibit a noticeable shift, indicating was no intermolecular interaction between PTX and P188 (Fig. 3B, black arrow). In contrast, the CO–NH in SDs shifted to the blue (Fig. 3B, red arrow) from 1652.89 to 1642.99 cm^{-1} with increased P188 (Fig. 3E), indicating a possible hydrogen bonding interaction (N–H···O) between PTX and P188 molecules in SD [26].

NMR is a highly sensitive and reliable tool for demonstrating complex formation and interactions between molecules [27]. In the case of drug-polymer interactions, the formation of hydrogen bonds weakens the shielding effect of electrons against hydrogen-bonded protons, leading to an increase in their chemical shift. Experimental results showed (Fig. 3C, D) showed that the proton H in CO–NH groups underwent a red shift to 7.09 ppm from 7.03 ppm with decreasing drug loading (Fig. 3F). The NH peak was a doublet due to the shift of linked C–H groups with the influence of the electron cloud density of NH groups [28].

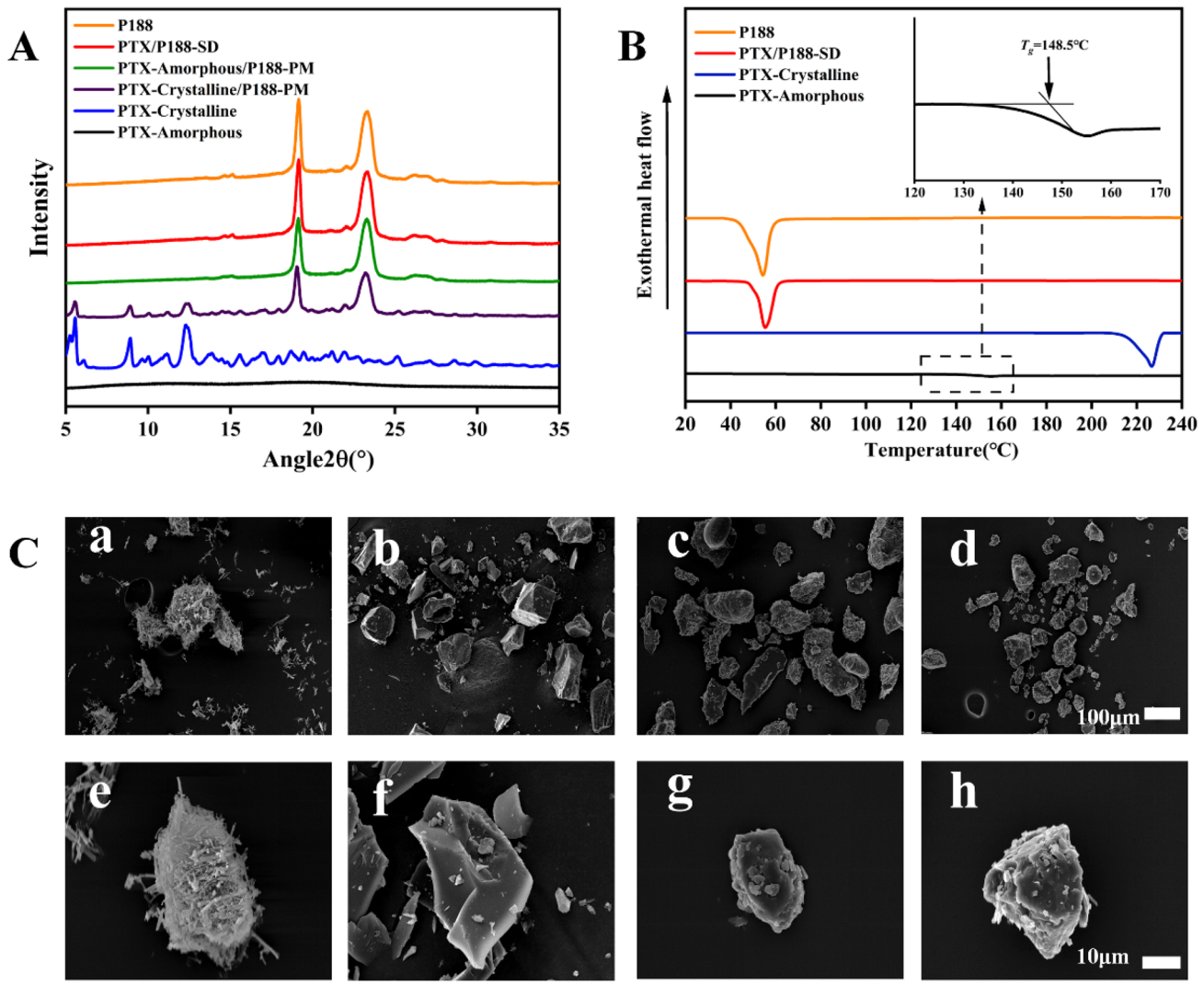

Fig. 2 Characterization of SD formulation. **A** PXRD profiles of P188, PTX (crystalline and amorphous), PM, and SD; **B** DSC profiles of P188 (crystalline and amorphous), PTX, and SD; **C** macroscopic SEM images, crystalline PTX (a and e), amorphous PTX (b and f), SD (c and g), and P188 (d and h). The scale bars for a, b, c, and d were 100 μm, and the scale bars for e, f, g, and h were 10 μm

The strength of the drug-polymer interaction is dependent on the ratio of the two components, and measuring the degree of peak shift allows for determination of the interaction strength, a mechanism that has been reported in the literature [29].

Both NMR and FT-IR experiments confirmed the existence of strong hydrogen bonding interactions between PTX and P188 molecules.

Solubility parameter

In previous studies, we have confirmed the presence of strong hydrogen bonding interactions between PTX and P188 molecules. However, it is still necessary to determine whether PTX interacts more strongly with the PPO segment or the PEO segment in P188. The compatibility between drugs and polymers can be predicted by calculating the solubility parameter values ($\Delta\delta_t$). It is generally believed that when $\Delta\delta_t$ ($MPa^{0.5}$) < 7, the drug has good compatibility with the polymer, and the smaller the value, the better the compatibility. When $\Delta\delta_t$ ($MPa^{0.5}$) > 10, the compatibility between the drug and polymer is considered to be poor [30]. As P188 is a triblock copolymer in which the PEO segments are in a stable crystalline state and the PPO segments are in an amorphous state, this study used PEG (100% PEO) and PPG (100% PPO) to simulate different portions of P188 for theoretical solubility parameter calculations. Using the group contribution method ($\Delta\delta_t$/$MPa^{0.5}$), the total solubility parameters of PTX, P188, PEG, and PPG were calculated as 26.44 (J

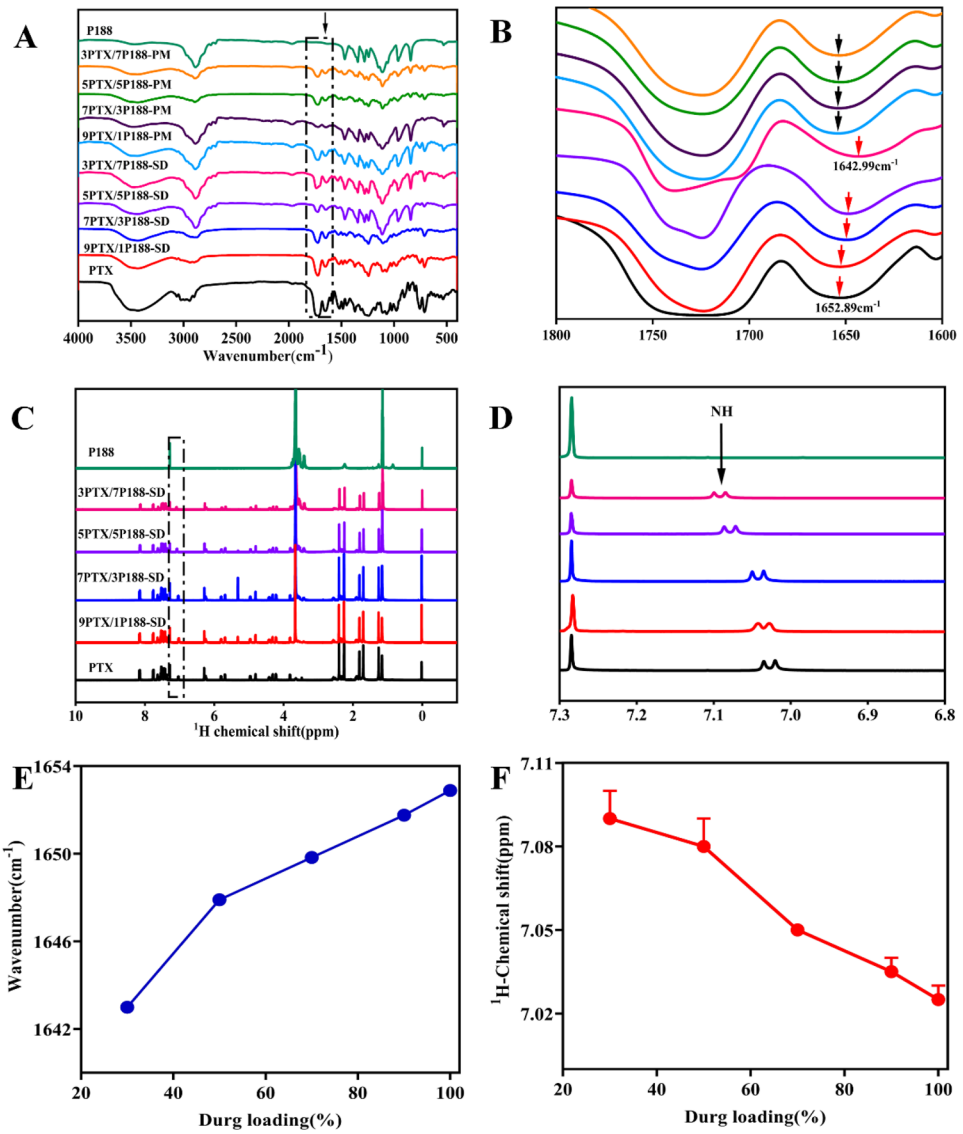

Fig. 3 Spectra of PTX, P188, and PTX/P188 systems. **A** FT-IR spectra of PTX, P188, PM, and SD; **B** characteristic peak shift spectra of FT-IR; **C** ^{1}H-NMR spectra of PTX, P188, PM, and SD; **D** characteristic peak shift spectra of ^{1}H-NMR; **E** comparison of CO–NH shifts in FT-IR; **F** comparison of NH group proton H shifts in ^{1}H-NMR

$cm^{-3})^{1/2}$, 20.80 (J $cm^{-3})^{1/2}$, 21.05 (J $cm^{-3})^{1/2}$, and 23.60 (J $cm^{-3})^{1/2}$, respectively. The overall solubility parameters of PTX with P188, PEG, and PPG resulted in $\Delta\delta_t$ values of 5.64 (J $cm^{-3})^{1/2}$, 5.39 (J $cm^{-3})^{1/2}$, and 2.84 (J $cm^{-3})^{1/2}$, respectively. Therefore, it can be concluded that PTX has the best compatibility with the PPO segments in P188 (Table 1).

Table 1 Solubility parameters for PTX, P188, PEG, and PPG

Drug/Polymer	δ_d/MPa$^{0.5}$	δ_p/MPa$^{0.5}$	δ_h/MPa$^{0.5}$	δ_t/MPa$^{0.5}$	$\Delta\delta$
PTX	26.15	3.85	0.46	26.44	N/A
P188	20.78	0.77	0.09	20.80	5.64
PEG	21.03	0.83	0.10	21.05	5.39
PPG	19.73	12.90	1.58	23.60	2.84

Interaction force parameters χ value

According to Flory–Huggins solution theory, drug-polymer interaction is a critical parameter in evaluating the system homogeneity. χ values are constant thermodynamic values determined by the chemical structure of the drug and polymer. When $\chi < 0$, the drug-polymer interaction is stronger than the drug-drug interaction, indicating good miscibility of the drug-polymer system. Conversely, when $\chi > 0$, the drug tends to aggregate by itself in the system, resulting in phase separation and poor miscibility [31]. In this study, equilibrium melting temperature (Tc, onset) and Flory–Huggins interaction parameters were detected at different scan rates after mixing PTX with P188, PEG, and PPG. The interaction parameters between PTX and P188, PEG, and PPG yielded χ values of − 1.9, − 4.7, and − 6.4,

respectively, which were consistent with the theoretical values of the solubility parameters.

To further confirm the distribution of PTX in P188, H1-NMR was employed to study the interaction of PTX in the PPO and PEG segments. The results showed that the chemical shifts of NH in PTX all changed with different of drug loadings, and the chemical shift of NH in PPO-PTX (Fig. 4C, D) was stronger than that in PEG-PTX (Fig. 4A, B) after mixing PTX with the polymer (Fig. 4E). Combining the results of the solubility parameter and interaction force parameters, it can be inferred that the interaction of PTX with the PPO segment is stronger than that with the PEG segment. Combining this result with the DSC result that only one Tg was detected in the SD indicates that the amorphous PTX mainly exists in the amorphous PPO segment in P188. To gain a more holistic view of the distribution of the drug between the three lamellae of the polymer, a physical schematic is illustrated (Fig. 4F).

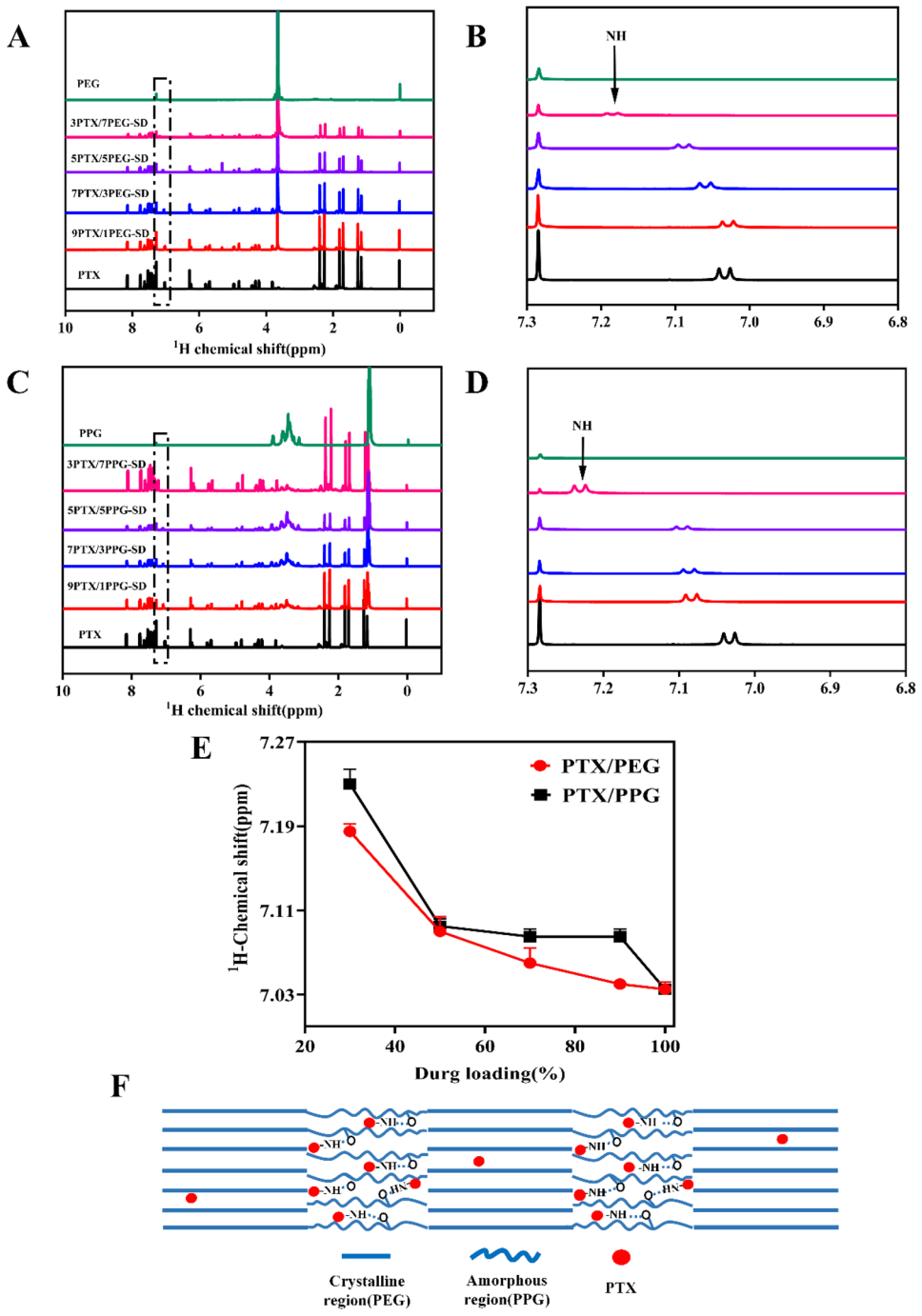

Fig. 4 **A** and **B** H^1-NMR spectra of the PTX/PEG system; **C** and **D** H^1-NMR spectra of the PTX/PPG system; **E** chemical shift comparison of proton H in the PTX/PEG system and the PTX/PPG system; **F** physical schematic of drug distribution in triblock (PEO-PPO-PEO)

In vitro dissolution study

The aim of this study is to improve the in vitro and in vivo dissolution rates of PTX. Therefore, it is crucial to examine the dissolution behavior of SD, which can vary based on dissolution conditions such as dissolution medium, leakage conditions, and dissolution device. To investigate the dissolution behavior of SD, we measured the intrinsic dissolution rate (IDR), powder dissolution rate, and pH conversion two-step dissolution rate.

IDR, also known as characteristic dissolution rate, is strongly linked to drug release behavior in vivo [22]. Moreover, IDR is an essential indicator for understanding the impact of drug-polymer interactions on the initial drug release of SD. Compared to other dissolution experiments, the release surface area of IDR is fixed, which can prevent release from being influenced by drug aggregation and uneven particle size variables. We compared the IDR of pure crystalline and amorphous PTX and their PM with P188. As shown in Fig. 5A, the IDR of crystalline PTX and amorphous solid PTX was 0.0027 mg/cm^2/min and 0.0086 mg/cm^2/min, respectively. This is because amorphous drugs have higher internal energy than crystalline drugs. Therefore, preparing drugs in the amorphous state is an effective way to improve the dissolution rate of insoluble drugs and their oral bioavailability [32, 33].

The IDR of crystalline PM and amorphous PM with a drug loading of 30% was 0.2462 mg/cm^2/min and 1.1422 mg/cm^2/min, respectively, which showed a significant improvement compared to pure drugs. This indicates that P188, an amphoteric surfactant, improves the solubility and wettability of the drug. The IDR of SD was 3.0364 mg/cm^2/min, which increased by 1124-fold (crystalline state) and 353-fold (amorphous state) compared to the raw drug, respectively. As an amphiphilic surfactant widely used in the pharmaceutics industry, the presence of P188 can enhance the solubility and wettability of PTX, as demonstrated by the 28-fold increase in IDR of the crystalline PM. This result was also consistent with the increasing solubility of PTX with increasing P188 concentration (data not shown) [23].

Powder dissolution is a crucial parameter for evaluating the dissolution rate of SD and can help explore the relationship between in vitro and in vivo dissolution behavior of the formulation. The powder dissolution rate considers various factors such as particle size, surface area, and particle aggregation and can therefore provide a comprehensive evaluation of the dissolution rate. Our results showed that the SD powder rapidly dissolved in PBS at a pH of 7.4, with a cumulative release rate of PTX reaching about 70% after approximately 15 min, which was much higher than that of PM and API (Fig. 6A). Due to the solubilization and wetting effects of P188 in PM, the drug dissolution rate also increased. After 15 min, a plateau period appeared, with the highest cumulative release rate of about 24%. There was no significant difference between crystalline and amorphous drugs. Still, it was statistically significant compared to SD (Fig. 6B). The API dissolution reached equilibrium within about 10 min, with no significant difference between the crystalline and amorphous states.

PH conversion two-step dissolution aims to study the dissolution rate of drugs in the pH environment of the gastrointestinal tract, which is essential for evaluating the drug release behavior in vivo. In vivo, the pH of the stomach is about 1.4, and in the intestine, it is about 6.5. Therefore, this dissolution method simulates these pH conditions to provide a reference for evaluating drug release behavior. Additionally, the limited volume of gastric juice cannot fully dissolve insoluble drugs. Hence, pH conversion, two-step dissolution, and powder dissolution are performed under non-sink conditions to better simulate drug release in gastric juice (Fig. 7).

The results revealed that SD rapidly dissolved at pH = 1.4, similar to intrinsic dissolution. After tablet disintegration, the dissolution medium quickly released the drug, with a maximum dissolution concentration of 8.24 μg/mL and a cumulative dissolution rate of around 82%. Adjusting the dissolution medium's pH to 6.5 caused the concentration of PTX in SD to decrease due to changes in medium volume. Still, the cumulative dissolution rate remained essentially unchanged, reaching dissolution equilibrium. The total area under the curve (AUC$_{(0–5\ h)}$) of API, PM, and SD

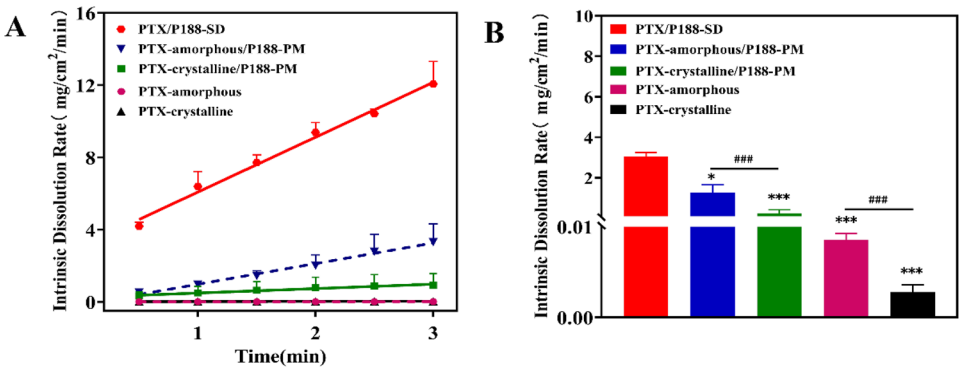

Fig. 5 IDR of PTX and SDs ($n = 3$). **A** IDR of SD, pure crystalline and amorphous PTX, and PM at pH = 1.4; **B** differential analysis of IDR. Compared with SD, $^{*}p < 0.05$, $^{***}p < 0.01$. Compared with pure crystalline PTX, $^{\#}p < 0.05$, $^{\#\#\#}p < 0.01$

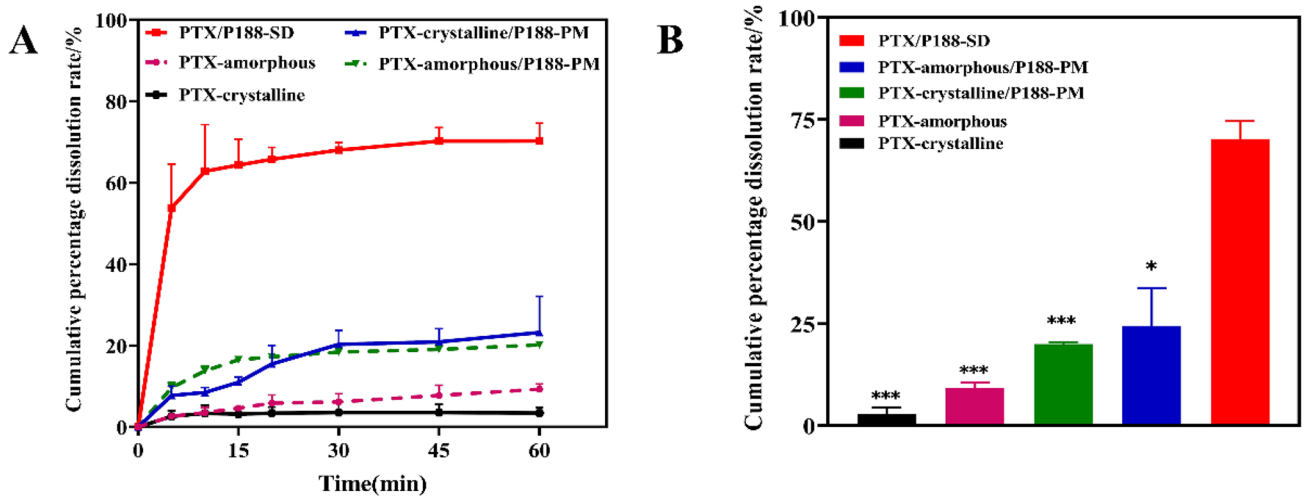

Fig. 6 Powder dissolution rate of PTX and SDs ($n=3$). **A** Powder dissolution rate of SD, pure crystalline and amorphous PTX, and PM at pH 7.4. Crystalline and amorphous PTX upon their physical mixture with P188 in phosphate buffer (PBS) ($n=3$); **B** differential analysis of powder dissolution rate. Compared to SD, $*p<0.05$, $***p<0.01$

was 51.86 ± 3.07 (μg/mL/h), 102 ± 5.92 (μg/mL/h), and 363.7 ± 8.21 (μg/mL/h), respectively. This is 7 times and 3.6 times that of API and PM, respectively. Regardless of the concentration and cumulative dissolution rate after dissolution, SD was superior to the raw drug and PM.

The dissolution of SD involves two critical steps: firstly, drug dissolution enters the dissolution medium to generate a certain level of supersaturation (the "spring" step). Secondly, the supersaturated drug maintains its supersaturation in polymer solutions (the "parachute" step) [32, 34]. It is crucial to study the process of generating and maintaining supersaturation in SD. The initial dissolution rate of a drug determines its ability to produce supersaturation (C_{max}), which can be explained by the IDR in this study. Furthermore, the ability to maintain supersaturation should also be examined, which is achieved through the powder dissolution experiment conducted in this study. A suitable SD formulation must strike a balance between the "spring" and "parachute" steps to ensure that the drug maintains a good physical state during dissolution and absorption. Finally, studying the critical factors that control the initial dissolution rate of drugs can aid in adjusting the dissolution and precipitation process of drugs in the preparation design process, which can enhance the oral bioavailability of drugs [35, 36].

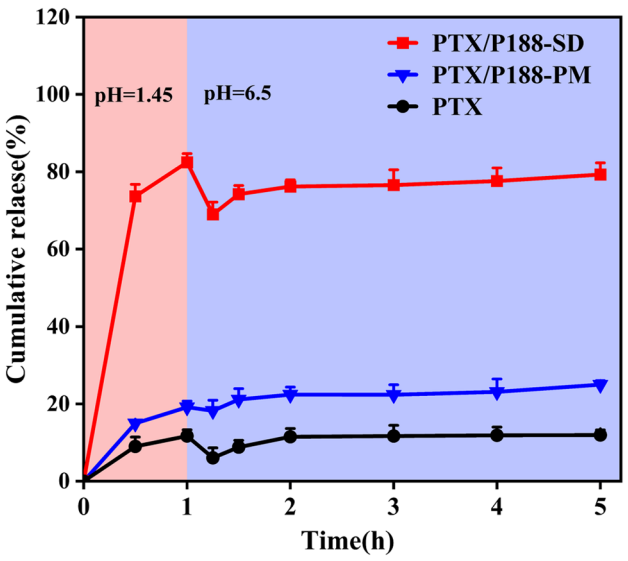

Fig. 7 The pH conversion two-step dissolution of PTX, PM, and SD ($n=3$)

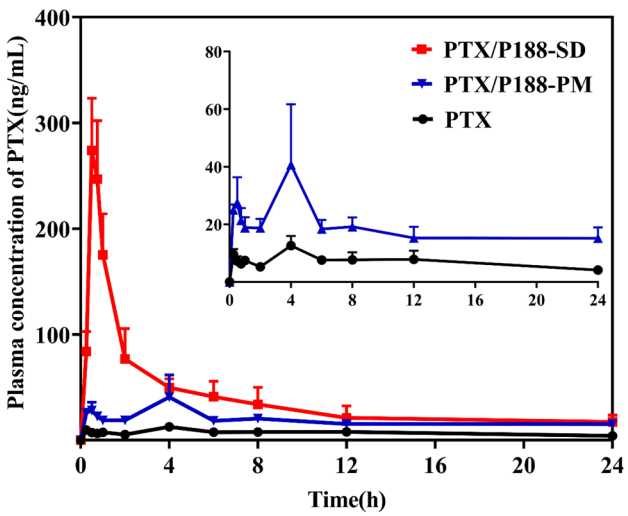

Fig. 8 Drug release behavior of the PTX formulation in vivo ($n=10$)

Table 2 Pharmacokinetics parameters of SD in vivo

Parameters	PTX	PM	SD
$AUC_{(0-24)}$ (ng/mL/h)	234.54 ± 142.10	321.07 ± 166.84	1438.82 ± 302.00
$AUC_{(0-\infty)}$ (ng/mL/h)	301.30 ± 188.45	541.64 ± 290.80	1712.10 ± 612.63
C_{max} (ng/mL)	17.91 ± 5.47	47.86 ± 28.83	357.51 ± 125.54
T_{max} (hours)	4.34 ± 2.60	4.08 ± 2.55	2.52 ± 4.00
$t_{1/2}$ (hours)	4.50 ± 3.94	5.22 ± 3.83	4.98 ± 3.67
$CL_{z/F}$ (L/h/kg)	0.24 ± 0.23	0.14 ± 0.11	0.04 ± 0.03
$MRT_{(0-24)}$ (hours)	8.71 ± 3.01	8.91 ± 2.74	7.85 ± 3.85
$MRT_{(0-\infty)}$ (hours)	9.09 ± 6.41	13.31 ± 4.83	8.51 ± 7.50

Pharmacokinetic comparison in Wistar rat

To assess the in vivo absorption of SD, the pharmacokinetics of PTX in male and female Wistar rats were evaluated after oral administration. The plasma concentration–time curve and pharmacokinetic parameters of PTX are depicted in Fig. 8 and Table 2, respectively.

The findings demonstrated that SD exhibited the highest oral absorption, with an $AUC_{(0-24)}$ of 1438.82 ± 302.00 (ng/mL/h). This is a sixfold and 4.5-fold increase in $AUC_{(0-24)}$ compared to API and PM, respectively, which correlates well with the in vitro pH conversion two-step dissolution. The C_{max} of SD was 357.51 ± 125.54 (ng/mL), which was nearly 7.6 and 20 times higher than that of PM (47.86 ± 28.83 ng/mL) and API (17.91 ± 5.47 ng/mL), respectively. In a study conducted by Miao et al. [23], the formulation with 15% P188 exhibited better absorption than the one lacking P188. This is attributed to P188, a widely used surfactant that enhances drug wettability, thereby increasing solubility. Furthermore, P188 can decrease the activity of P-GlycoProtein (Pgp) through various mechanisms and increase the oral permeability of various Pgp substrates, such as rifampicin and ranitidine [37, 38]. In another study by Johanna, P188 was used as a carrier to enhance the permeability of loperamide on Pgp-expressing epithelial cells [39]. As PTX is a BCS IV drug and Pgp efflux substrate, P188 can inhibit the activity of Pgp and modify cell permeability, which could be the primary reason for the favorable absorption of PTX-SD in this study, using P188 as the carrier.

In this study, the T_{max} of SD was observed to be nearly 1.5 h earlier than that of PTX, with PM also showing a slightly earlier T_{max}. This may be because most small molecule drugs enter the bloodstream via passive transmembrane mechanisms through the gastrointestinal tract [39], and the rate of transmembrane transport is affected by the drug concentration difference on both sides of the cell membrane and the cell membrane permeability. As demonstrated in this study, the drug release rate in SD is much higher than in PM, leading to a larger drug concentration difference on both sides of the cell membrane. Additionally, P188 has been reported to improve the permeability of intestinal epithelial cells, thereby increasing oral absorption. For example, Poloxamer 188-Coated Ammonium Methacrylate Copolymer Nanocarriers have been shown to enhance loperamide permeability across Pgp-expressing epithelia [39]. Thus, SD with P188 as the carrier can significantly accelerate the absorption rate of PTX. Finally, it should be noted that there was no gender difference observed in the oral absorption of SD in male and female rats in this study. There is an abnormal phenomenon that needs to be explained. In the PK experiment, we found that the concentration time curve of PTX raw material and physical mixture showed a bimodal phenomenon around 1 h. But there are no such reports in other literature. Through reviewing the original data and literature, we found that this phenomenon was due to the large error of individual data, which led to the deviation of the average value, but this deviation would not affect our judgment on the bioavailability results. So in order to ensure the integrity and authenticity of the data, we did not discard data with significant deviations.

Conclusion

In this study, we utilized a spray drying technology with poloxamer 188 as the carrier to prepare a solid dispersion of paclitaxel (PTX-SD), to enhance its dissolution rate and oral bioavailability.

Our investigation of the microstructure of PTX-SD was completed through three approaches: (1) PXRD and DSC confirmed that PTX exists in an amorphous state within SD, while P188 is crystalline. We then explored why amorphous PTX can form a solid dispersion with crystalline P188. (2) IR and H^1-NMR results demonstrated intermolecular interaction between the NH bond of PTX and the OH bond of P188, which we determined to be hydrogen bonding. Given that P188 is a triblock copolymer containing PEO-PPO-PEO segments, we utilized solubility parameters, interaction force parameters, and H^1-NMR technology to confirm that PTX interacts more strongly with the PPO chain segments of P188, revealing that PTX is more inclined to bind with PPO segments in P188 and explaining the formation of the solid

dispersion. To assess the improved dissolution rate and bioavailability of PTX, we conducted in vitro dissolution tests using three different models and a pharmacokinetic study. Our results showed that the $AUC_{(0–24\ h)}$ of SD was 6 times higher than that of API, 4.5 times higher than that of PM, and C_{max} was nearly 20 times higher than that of API. These outcomes can be attributed to the increased dissolution rate of amorphous PTX and changes in cell membrane permeability caused by P188.

Our findings indicate that PTX-SD, prepared with P188 as the carrier, can effectively enhance the dissolution rate and oral bioavailability of PTX.

Author contribution Conceptualization, experimental work, writing (draft), and writing revision: YL; experimental work and writing (draft): YZ; experimental work: QL.Y; and conceptualization and manuscript revision: XP.Z and CH.H.

Funding This research was supported by the science and technology of Qinghai Province (No. 2022-QY-201) and the National Natural Science Foundation of China (Project No. 82060644).

Availability of data and materials The datasets used or analyzed during the current study are available from the corresponding author upon reasonable request.

Declarations

Ethics approval and consent to participate All animal study protocols were approved by the Institutional Animal Care and Utilization Committee of Qinghai University, CAS (approval numbers -QHU -IPC -23041).

Consent for publication Not applicable. No human studies have been performed in this research.

Competing interests The authors declare no competing interests.

References

1. Della CL, Barra F, Foreste V, Giampaolino P, Evangelisti G, Ferrero S, Bifulco G. Advances in paclitaxel combinations for treating cervical cancer. Expert Opin Pharmacother. 2020;21(6):663–77.
2. Fasching PA, Link T, Hauke J, Seither F, Jackisch C, Klare P, Schmatloch S, Hanusch C, Huober J, Stefek A, Seiler S, Schmitt WD, Uleer C, Doering G, Rhiem K, Schneeweiss A, Engels K, Denkert C, Schmutzler RK, Hahnen E, Untch M, Burchardi N, Blohmer JU, Loibl S. Neoadjuvant paclitaxel/olaparib in comparison to paclitaxel/carboplatinum in patients with HER2-negative breast cancer and homologous recombination deficiency (GeparOLA study). Ann Oncol. 2021;32(1):49–57.
3. Okada T, Okamoto I, Sato H, Ito T, Miyake K, Tsukahara K. Efficacy and safety of paclitaxel combined with cetuximab for head and neck squamous cell carcinoma. In Vivo. 2021;35(2):1253–9.
4. Hu Y, Zhang K, Zhu X, Zheng X, Wang C, Niu X, Jiang T, Ji X, Zhao W, Pang L, Qi Y, Li F, Li L, Xu Z, Gu W, Zou H. Synergistic inhibition of drug-resistant colon cancer growth with PI3K/mTOR dual inhibitor BEZ235 and nano-emulsioned paclitaxel via reducing multidrug resistance and promoting apoptosis. Int J Nanomedicine. 2021;16:2173–86.
5. Alves RC, Fernandes RP, Eloy JO, Salgado HRN, Chorilli M. Characteristics, properties and analytical methods of paclitaxel: a review. Crit Rev Anal Chem. 2018;48(2):110–8.
6. Tran P, Park J. Formulation of solid dispersion to improve dissolution and oral bioavailability of poorly soluble dexibuprofen. Pharm Dev Technol. 2021;26(4):422–30.
7. Vinarov Z, Katev V, Radeva D, Tcholakova S, Denkov ND. Micellar solubilization of poorly water-soluble drugs: effect of surfactant and solubilizate molecular structure. Drug Dev Ind Pharm. 2018;44(4):677–86.
8. Du J, Li X, Zhao H, Zhou Y, Wang L, Tian S, Wang Y. Nanosuspensions of poorly water-soluble drugs prepared by bottom-up technologies. Int J Pharm. 2015;495(2):738–49.
9. Zhang Z, Mei L, Feng S. Paclitaxel drug delivery systems. Expert Opin Drug Deliv. 2013;10(3):325–40.
10. Rahman M, Son M, Kim H, Lee I, Jeon H, Kim M, Kwon H, Park S, Jang J, Kim S. DHP107, a novel oral paclitaxel formulation induces less peripheral neuropathic pain and pain-related molecular alteration than intravenous paclitaxel preparation in rat. J Adv Biotechnol Exp Ther. 2019;2(2):55–64.
11. Kim S, Seo JH, Ahn J, Kim T, Kang SY, Sohn J, Yang Y, Park KH, Moon YW, Lim S, Kang MJ, Yoon KE, Cho HJ, Lee KS. Phase II study of DHP107 (oral paclitaxel) in the first-line treatment of HER2-negative recurrent or metastatic breast cancer (OPTIMAL study). Ther Adv Med Oncol. 2021;13:1–11.
12. Sekiguchi K, Obi N. Studies on absorption of eutectic mixture. I. A comparison of the behavior of eutectic mixture of sulfathiazole and that of ordinary sulfathiazole in man. Chem Pharm Bull. 1961;9(11):866–72.
13. Altamimi MA, Neau SH. Investigation of the in vitro performance difference of drug-Soluplus® and drug-PEG 6000 dispersions when prepared using spray drying or lyophilization. Saudi Pharma J. 2017;25(3):419–39.
14. Reddy RK, Khalil SA, Wafik GM. Effect of dioctyl sodium sulfosuccinate and poloxamer 188 on dissolution and intestinal absorption of sulfadiazine and sulfisoxazole in rats. J Pharm Sci. 1976;65(1):115–8.
15. Sharma A, Jain CP, Tanwar YS. Preparation and characterization of solid dispersions of carvedilol with poloxamer 188. J Chil Chem Soc. 2013;58(1):1553–7.
16. Gorajana A, Rajendran A, Yew L, Dua K. Preparation and characterization of cefuroxime axetil solid dispersions using hydrophilic carriers. Int J Pharm Investig. 2015;5(3):171–8.
17. Hu C, Liu Z, Liu C, Zhang Y, Fan H, Qian F. Improvement of antialveolar echinococcosis efficacy of albendazole by a novel nanocrystalline formulation with enhanced oral bioavailability. ACS Infect Dis. 2020;6(5):802–10.
18. Qian F, Tao J, Desikan S, Hussain M, Smith RL. Mechanistic investigation of Pluronic® based nano-crystalline drug-polymer solid dispersions. Pharm Res. 2007;24(8):1551–60.
19. Mohammad MA, Alhalaweh A, Velaga SP. Hansen solubility parameter as a tool to predict cocrystal formation. Int J Pharm. 2011;407(1):63–71.
20. Sun Y, Tao J, Zhang GGZ, Yu L. Solubilities of crystalline drugs in polymers: an improved analytical method and comparison of solubilities of indomethacin and nifedipine in PVP, PVP/VA, and PVAc. J Pharm Sci. 2010;99(9):4023–31.
21. Shanmugam S, Im HT, Sohn YT, Kim Y, Park J, Park E, Woo JS. Enhanced oral bioavailability of paclitaxel by solid dispersion granulation. Drug Dev Ind Pharm. 2015;41(11):1864–76.
22. Chen Y, Wang S, Wang S, Liu C, Su C, Hageman M, Hussain M, Haskell R, Stefanski K, Qian F. Initial drug dissolution from amorphous solid dispersions controlled by polymer dissolution and drug-polymer interaction. Pharm Res. 2016;33(10):2445–58.
23. Miao L, Liang Y, Pan W, Gou J, Yin T, Zhang Y, He H, Tang X. Effect of supersaturation on the oral bioavailability of paclitaxel/

polymer amorphous solid dispersion. Drug Deliv Transl Res. 2019;9(1):344–56.
24. Liggins RT, Hunter WL, Burt HM. Solid-state characterization of paclitaxel. J Pharm Sci. 1997;86(12):1458–63.
25. Choi J, Cho NH, Kim D, Park J. Comparison of paclitaxel solid dispersion and polymeric micelles for improved oral bioavailability and in vitro anti-cancer effects. Mater Sci Eng, C. 2019;100:247–59.
26. Weyna DR, Cheney ML, Shan N, Hanna M, Wojtas A, Zaworotko MJ. Crystal engineering of multiple-component organic solids: pharmaceutical cocrystals of tadalafil with persistent hydrogen bonding motifs. CrystEngComm. 2012;14(7):2377–80.
27. Baghel S,Cathcart H, O'Reilly NJ. Understanding the generation and maintenance of supersaturation during the dissolution of amorphous solid dispersions using modulated DSC and 1H NMR. Int J Pharm. 2018;536(1):414–25.
28. Gao D, Zhu D, Zhou X, Dong S, Chen Y. Inhomogeneous phase significantly reduces oral bioavailability of felodipine/PVPVA amorphous solid dispersion. Mol Pharm. 2023;20(1):409–18.
29. Chen Y, Liu C, Chen Z, Su C, Hageman M, Hussain M, Haskell R, Stefanski K, Qian F. Drug–polymer–water interaction and its implication for the dissolution performance of amorphous solid dispersions. Mol Pharm. 2015;12(2):576–89.
30. Mukesh S, Joshi P, Bansal AK, Kashyap MC, Mandal SK, Sathe V, Sangamwar AT. Amorphous salts solid dispersions of celecoxib: enhanced biopharmaceutical performance and physical stability. Mol Pharm. 2021;18(6):2334–48.
31. Qian F, Huang J, Hussain MA. Drug–polymer solubility and miscibility: stability consideration and practical challenges in amorphous solid dispersion development. J Pharm Sci. 2010;99(7):2941–7.
32. Brouwers J, Brewster ME, Augustijns P. Supersaturating drug delivery systems: the answer to solubility-limited oral bioavailability? J Pharm Sci. 2009;98(8):2549–72.
33. Leuner C, Dressman J. Improving drug solubility for oral delivery using solid dispersions. Eur J Pharm Biopharm. 2000;50(1):47–60.
34. Guzman HR, Tawa M, Zhang Z, Ratanabanangkoon P, Shaw P, Gardner CR, Chen H, Moreau JP, Almarsson O, Remenar JF. Combined use of crystalline salt forms and precipitation inhibitors to improve oral absorption of celecoxib from solid oral formulations. J Pharm Sci. 2007;96(10):2686–702.
35. Liu C, Chen Z, Chen Y, Lu J, Li Y, Wang S, Wu G, Qian F. Improving oral bioavailability of sorafenib by optimizing the "spring" and "parachute" based on molecular interaction mechanisms. Mol Pharm. 2016;13(2):599–608.
36. Sun DD, Lee PI. Probing the mechanisms of drug release from amorphous solid dispersions in medium-soluble and medium-insoluble carriers. J Control Release. 2015;211:85–93.
37. Alakhova DY, Kabanov AV. Pluronics and MDR reversal: an update. Mol Pharm. 2014;11(8):2566–78.
38. Ma L, Wei Y, Zhou Y, Ma X, Wu X. Effects of Pluronic F68 and Labrasol on the intestinal absorption and pharmacokinetics of rifampicin in rats. Arch Pharm Res. 2011;34(11):1939–43.
39. Catalan-Figueroa J, Garcia MA, Contreras P, Boisset CB, Gonzalez PM, Fiedler JL, Perez MF, Morales JO. Poloxamer 188-coated ammonium methacrylate copolymer nanocarriers enhance loperamide permeability across Pgp-expressing epithelia. Mol Pharm. 2021;18(2):743–50.